Supplementary Materials:

Cryogenic tribological breakthroughs in medium-entropy alloy composites via regulated partial recrystallization

Yue Ren[1, 2, †], Longhui Zhu[1, †], Yusen Li[3], Qing Zhou[1,*], Stefan J. Eder[4], Xudong Sui[4,*], Qingfeng Wu[1], Haifeng Wang[1,*], Zhijun Wang[1], Carsten Gachot[4], Jian Wang[5], Weimin Liu[1, 6]

[1] State Key Laboratory of Solidification Processing, Center of Advanced Lubrication and Seal Materials, Northwestern Polytechnical University, Xi'an 710072, PR China

[2] Automotive Engineering Research Institute, Byd Auto Industry Company Limited, Shenzhen 518000, PR China

[3] Sino-French Institute of Computing Technology for Advanced Materials (CTAM), B.P. 2060, 10010 Troyes cedex, France

[4] Institute of Engineering Design and Product Development, Research Unit Tribology, TU Wien, Vienna, Austria

[5] Mechanical and Materials Engineering, University of Nebraska-Lincoln, Lincoln, NE, 68588, USA

[6] State Key Laboratory of Solid Lubrication, Lanzhou Institute of Chemical Physics, Chinese Academy of Sciences, Lanzhou 730000, PR China

[†] These authors contributed equally to this work.

* Corresponding author's e-mail: zhouqing@nwpu.edu.cn (Q. Zhou); xudong.sui@tuwien.ac.at (X. Sui); haifengw81@nwpu.edu.cn (H. Wang)

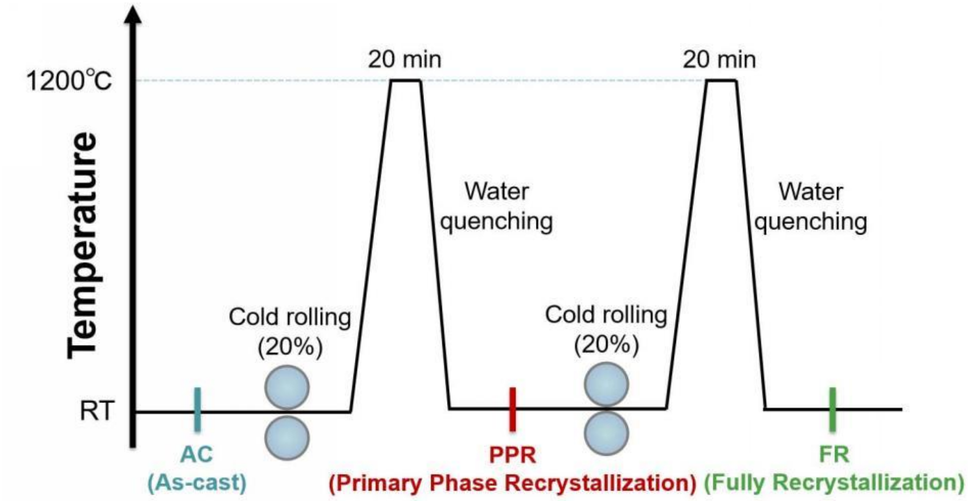

Fig. S1. Schematic procedures for processing the as-cast (AC) MEA, the primary phase recrystallization (PPR) MEA and the fully recrystallization (FR) MEA.

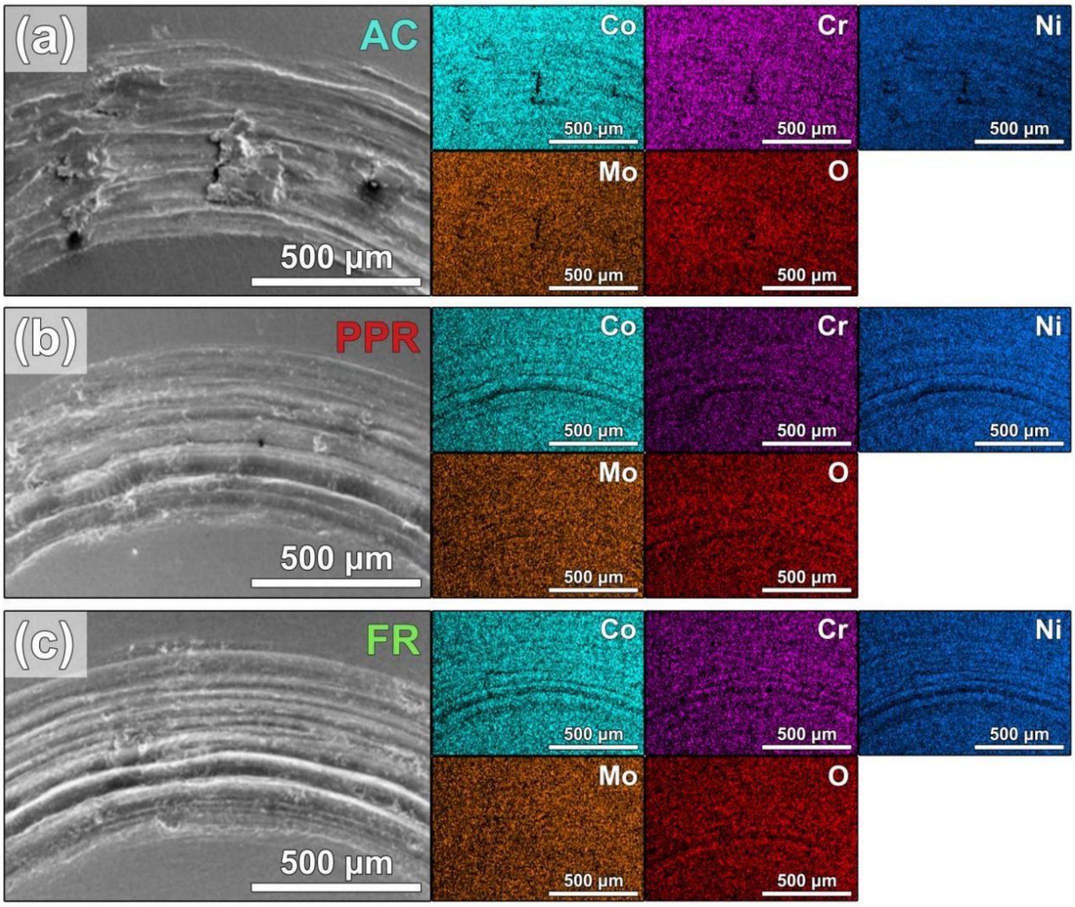

Fig. S2. EDS analyses of worn surface after wear tests at 113 K of (a) the AC, (b) the PPR, and (c) the FR MEAs.

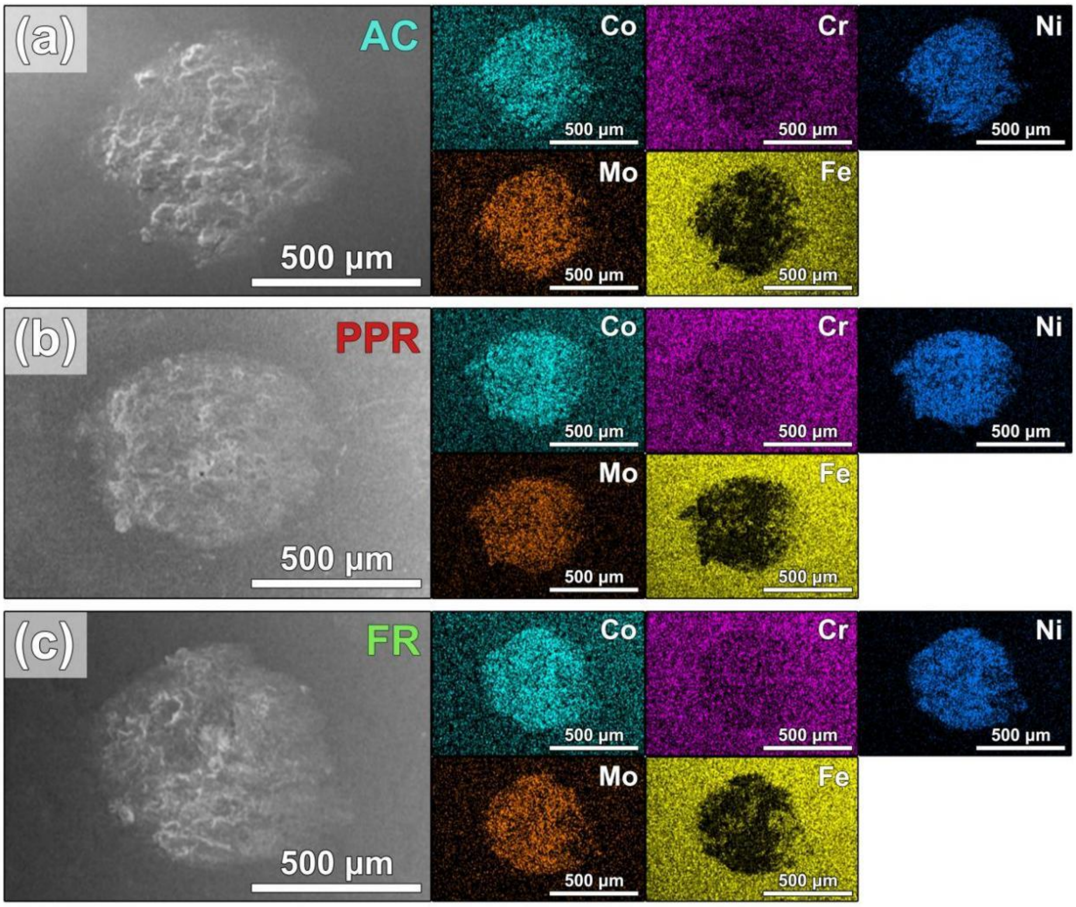

Fig. S3. EDS analyses of counterbody after wear tests at 113 K with (a) the AC, (b) the PPR, and (c) the FR MEAs.

1. Mechanical analysis of FEM

The choice of an appropriate constitutive model is critical for accurate numerical simulation of composite behavior. In general, a constitutive model consists of two main components: a hardening law and a failure criterion. The hardening law describes the stress–strain relationship in the plastic regime, while the failure criterion defines damage evolution and predicts the onset of material failure. Different materials exhibit distinct mechanical responses under load, necessitating tailored constitutive models for each case. Accurate finite element simulations can only be achieved by selecting a constitutive model that captures the material's behavior including damage. Therefore, a key aspect of this study is identifying suitable damage-inclusive constitutive models for both the composite material and the layer interfaces.

In the description of the constitutive model, the elastic deformation phase is governed by Hooke's Law. The plastic hardening phase, however, is more complex and can be described in various ways within ABAQUS. In this study, the Ludwik flow criterion is employed to characterize the plastic hardening behavior [5]:

$$\sigma = \sigma_0 + K(\overline{\varepsilon}^p)^n \tag{1}$$

where σ is the flow stress, σ_0 is the yield stress, $\overline{\varepsilon}^p$ is the equivalent plastic strain, K and n is the hardening parameters. During the material hardening phase, plastic strain accumulates continuously. The ductile damage of the FCC matrix was taken into consideration, and the stiffness degradation rate was used to describe the damage evolution behavior of the matrix. A damage factor $D(0 \le D \le 1)$ was introduced to express the decay process of the material, where 0 means no damage and 1 means a complete damage and failure. In this study, when the total accumulated strain reaches a critical value, as defined by Eq. (2), material damage initiates:

$$\int \frac{\Delta \varepsilon^p}{\varepsilon^p} = 1 \tag{2}$$

Other parameters of this model were approximately set as shown in Fig. S4.

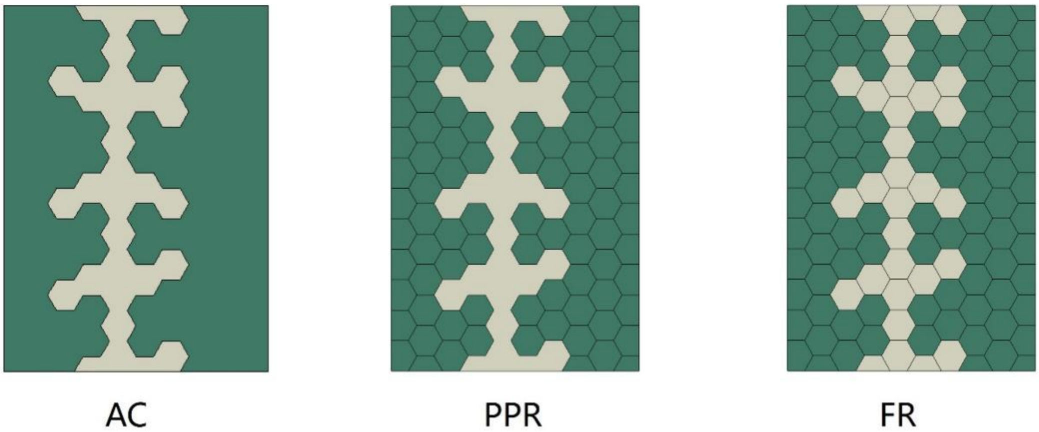

	Density(g/mm3)	Elastic modulus(MPa)	Yield strength(MPa)
FCC	8.2e-09	200 000	500
SIGMA	8.8e-09	250 000	1500

	FCC-FCC (MPa)	FCC-σ (MPa)	σ-σ (MPa)
Interface strength	1500	1000	800

Fig. S4. Models and parameters for finite element simulations. The origin of the data selection can be found in [1-4].

In this study, element-based cohesive approach was adopted to predict the traction-separation behavior of the interface. The elastic phase of the cohesive model is linear elastic, while the stiffness degradation phase can adopt either linear or exponential forms. This study employs linear degradation to depicts the damage evolution process of the cohesive element, as shown in Fig. S5. The properties of the cohesive model are defined by the cohesive element stiffness k, maximum stress *t*, fracture energy *G*, and failure criteria. The tension-displacement relationship of the cohesive model is described by the following equations

$$\varepsilon_n = \frac{\delta_n}{T_0} \tag{3}$$

$$\varepsilon_s = \frac{\delta_s}{T_0} \tag{4}$$

$$t = \begin{Bmatrix} t_n \\ t_s \end{Bmatrix} = \begin{bmatrix} K_{nn} & \\ & K_{ss} \end{bmatrix} \begin{Bmatrix} \varepsilon_n \\ \varepsilon_s \end{Bmatrix} \tag{5}$$

In Eq. (3) and (4), ε_n represents the normal strain, δ_n denotes the normal crack opening displacement, ε_s is the shear strain, and δ_s is the shear crack opening displacement, with T_0 being the initial thickness of the cohesive element. In Eq. (5), K_{nn} and K_{ss} represent the normal and shear stiffness, respectively, and t is the stress tensor.

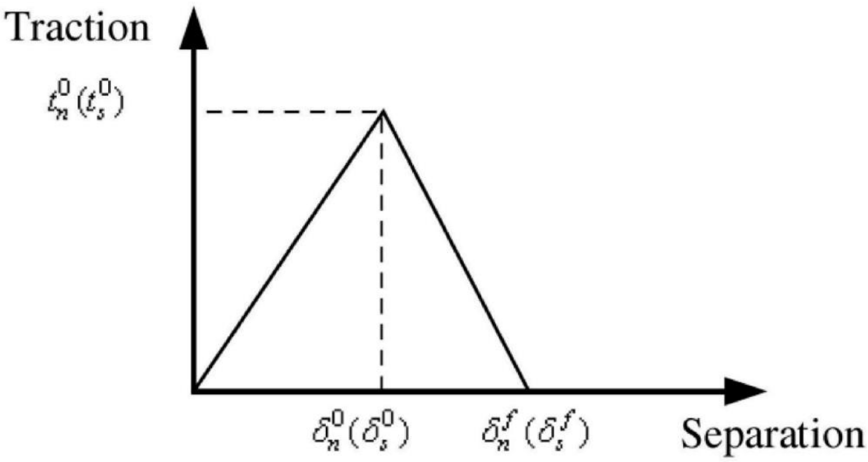

Fig. S5. Traction-separation model.

By introducing the damage variable D_1 to express the damage evolution of the interface, the evolution of the damage variable in ABAQUS is expressed as:

$$D_1 = \frac{\delta_m^f(\delta_m^{\max} - \delta_m^0)}{\delta_m^{\max}(\delta_m^f - \delta_m^0)} \tag{6}$$

where δ_m^0 indicates the displacement as the damage initiates, δ_m^f means the displacement as the damage complete, and $\delta_m^{\max}$ means the maximum displacement.

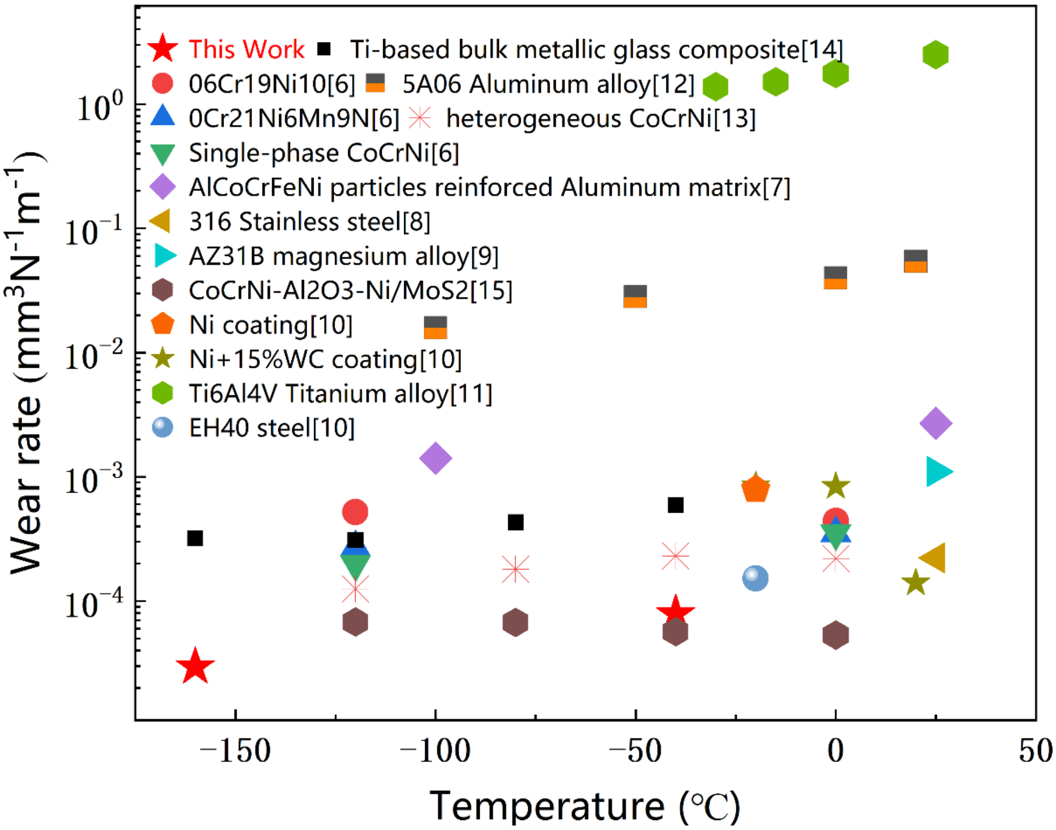

Fig. S6. The references for Fig. 4(c) are indicated and listed below. It should be noted that due to the differences in test environment conditions, the comparison conducted here is an approximate assessment of the material's wear performance.

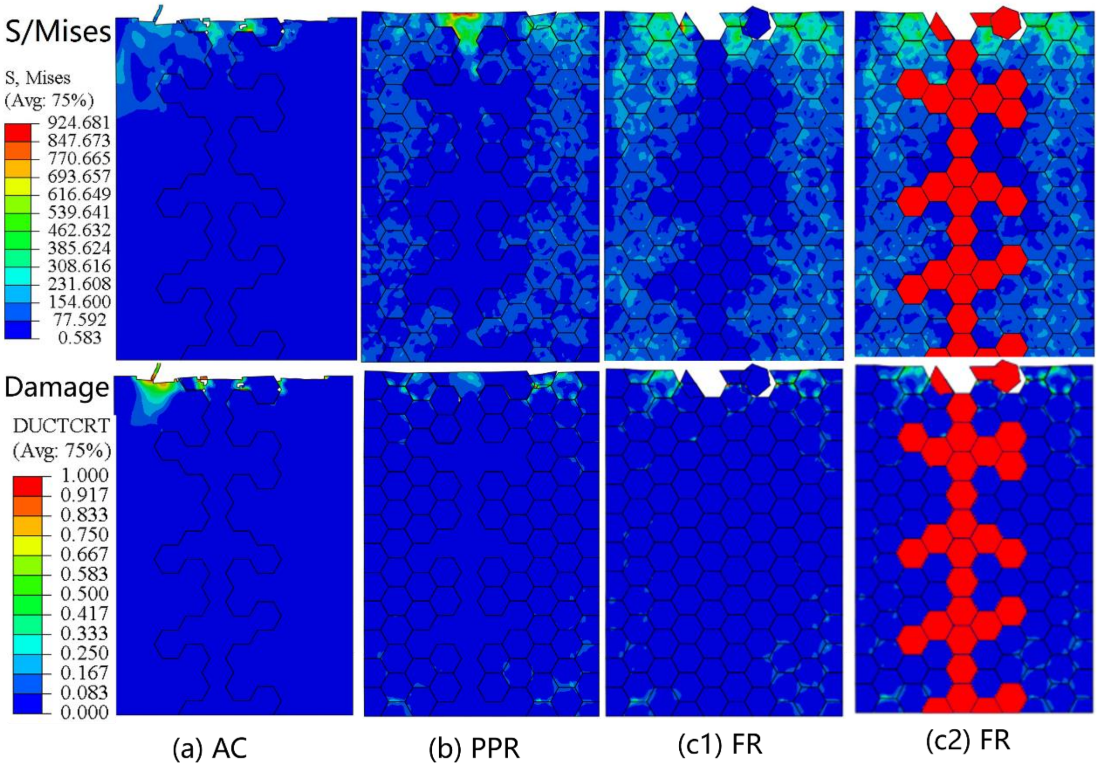

Fig. S7. Stress Distribution (S/Mises) and damage of different samples in the FEM.

References

[1] L.H. Liu, K.J. Lu, Z.Y. Jing, Z.B. Zhang, L. Xue, J.C. Yuan, X. Li, B.S. Zhang, X.B. Liang, J.B. Cheng, Simultaneously improving strength and corrosion resistance of CoCrNi-based multi-principal element alloys via alloying with Mo content. J. Alloy. Compd. 1010 (2025) 15.

[2] G. Laplanche, A. Kostka, C. Reinhart, J. Hunfeld, G. Eggeler, E.P. George, Reasons for the superior mechanical properties of medium-entropy CrCoNi compared to high-entropy CrMnFeCoNi. Acta Mater. 128 (2017) 292-303.

[3] N. Li, J. Gu, B. Gan, Q. Qiao, S. Ni, M. Song, Effects of Mo-doping on the microstructure and mechanical properties of CoCrNi medium entropy alloy. J. Mater. Res. 35(20) (2020) 2726-2736.

[4] L. Sun, Z. He, N. Jia, Local chemical order enables an ultrastrong and ductile high-entropy alloy in a cryogenic environment. Science Advances, 10(48) (2024): eadq6398.

[5] D. Wigley, Mechanical properties of materials at low temperatures. SSBM (2012).

[6] Y. Ren, Q. Zhou, D. Hua, et al. Wear-resistant CoCrNi multi-principal element alloy at cryogenic temperature. Sci. Bull. 69(2) (2024) 227-236.

[7] K. Luo, W. Farid, A. Fouly, et al. Tribological characterization of high entropy alloy particles reinforced aluminum matrix composites at room and cryogenic temperatures. Tribol. Int. 205 (2025) 110546.

[8] F.E. Kennedy, Y.X. Ye, I. Baker, et al. Development of a new cryogenic tribotester and its application to the study of cryogenic wear of AISI 316 stainless steel. Wear 496-497 (2022) 204309.

[9] C. Rathinasuriyan, R. Sankar. Wear and corrosion behavior of cryogenic friction stir processed AZ31B alloy. J. Mater. Eng. Perform. 30 (2021) 3118-3128.

[10] Q. Cao, L. Fan, H. Chen, et al. Wear behavior of laser cladded WC-reinforced Ni-based coatings under low temperature. Tribol. Int. 176 (2022) 107939.

[11] Y. Zhu, L. Song, Z. Deng, et al. Study of the Friction and Wear Behavior of Ti-6Al-4V Alloy Under Low Temperatures. JOM (2025) 1-12.

[12] T. Ye, Z. Jia, J. Ma, et al. Mechanical and tribological properties of 5A06 aluminum alloy at low temperature. Surf. Topogr.: Metrol. Prop. 11(1) (2023) 015011.

[13] Z. Huang, Y. Ren, D. Luo, et al. Improved wear resistance of a heterogeneous CoCrNi medium-entropy alloy at cryogenic temperature. Tribol. Lett. 70(4) (2022) 96.

[14] Y. Ren, T. Yan, Z. Huang, et al. Cryogenic wear behaviors of a metastable Ti-based bulk metallic glass composite. J. Mater. Sci. Technol. 134 (2023) 33-41.

[15] Y. Wang, Z. Jiao, Y. Shi, et al. Investigation on the wear performance of CoCrNi matrix self-lubricating composites at cryogenic temperature. Surf. Coat. Technol. 500 (2025): 131906.